Journal of Advances in Applied & Computational Mathematics, 2026, 134-149

Published by Avanti Publishers

Journal of Advances in Applied & Computational Mathematics

ISSN (online): 2409-5761

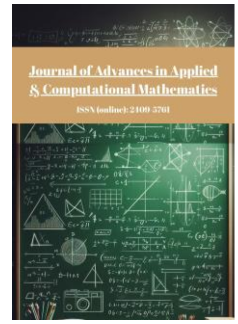

Magnetohydrodynamic Williamson Fluid Flow and Heat Transfer over a Stretching Cylinder with Variable Thermal Conductivity and Internal Heat Generation: A BVP4C Numerical Study

Muhammad Sohail* and Naeema Malik

Institute of Mathematics, Khwaja Fareed University of Engineering and Information Technology, Rahim Yar Khan 64200, Pakistan

ARTICLE INFO

Article Type: Research Article

Academic Editor: Youssef Raffoul

Keywords:
Williamson fluid
Stretching cylinder
Heat transfer enhancement
Variable thermal conductivity
Magnetohydrodynamic (MHD) flow

Timeline:
Received: July 23, 2026
Accepted: August 29, 2026
Published: September 15, 2026

Citation: Sohail M, Malik N. Magnetohydrodynamic Williamson fluid flow and heat transfer over a stretching cylinder with variable thermal conductivity and internal heat generation: A BVP4C numerical study. J Adv Appl Computat Math. 2026; 13(2): 134-149.

DOI: https://doi.org/10.15377/2409-5761.2026.13.8

ABSTRACT

This article's, the optimization of heat transfer from a stretching cylinder in a non-Newtonian Williamson fluid subjected to combined magnetohydrodynamic (MHD) forces, variable thermal conductivity, and internal heat generation is still a research mystery despite the extensive research efforts conducted on fluid transport. In order to get around this, appropriate similarity transformations are used to convert governing non-linear partial differential equations for mass, motion, and energy into non-dimensional ordinary differential equations. The 4th order collocation solver bvp4c in MATLAB is used to numerically solve the resulting non-linear boundary value system. For various values of the magnetic parameter (M), Weissenberg number (λ), curvature parameter (γ), Prandtl number ($\boldsymbol{Pr}$), thermal conductivity parameter (ε), and heat generation/absorption (β), the velocity and thermal boundary layer behavior are methodically examined. Increased values of the magnetic (M), and elastic(λ) parameters reduce fluid motion with the emergence of resistive Lorentz forces when compared to the other parameters, however increased values of (γ) greatly improve momentum transmission. Furthermore, the variable thermal conductivity (ε) and heat generation (β) result in a notable rise in the thickness of the thermal boundary layer and an increase in the core temperature profiles. These thermal quantitative measurements provide crucial design parameters for wire coating applications, thermal management systems, and polymer extrusion in industry.

*Corresponding Author
Email: muhammad_sohail111@yahoo.com

1. Introduction

In contemporary mechanical, chemical, and industrial engineering applications, modeling boundary layer transport phenomena of non-Newtonian fluids is crucial. Unlike conventional Newtonian models, which assume that viscosity is linearly related to shear rate, non-Newtonian fluids display complicated rheological features, such as stress-dependent viscosity. One of these models, the Williamson fluid, is frequently used to model pseudoplastic or shear-thinning fluids, where the fluid's viscosity drops as the shear rate increases. The fundamental rheological model for pseudoplastic fluids was initially created by Williamson [1]. The more intricate non-Newtonian representations were made possible by Hayat *et al*. [2] extending the analytical investigation of non-Newtonian properties to second-grade fluids. Williamson models over expanding sheets have recently been the subject of groundbreaking studies by Nadeem *et al*. [3] (as contextualized in the fundamental literature) and structurally examined at stagnation points by Nandeppanavar and Vajravelu [4]. In order to further this understanding, Khan [5] and Bilal [6] carried out higher order numerical analysis utilizing thermal stratification models and Runge-Kutta-Fehlberg (RKF) schemes to replicate the precise physical properties of these complex flows.

Although the flow over curved surfaces, such as extending cylinders, is susceptible to variations in complexity due to the curvature of the surfaces and the localized friction, early boundary layer research focused on planar arrangements. The physiological and industrial importance of cylindrical extensions has been extensively researched. Heat transfer profiles in non-Newtonian frameworks are significantly influenced by surface curvature, according to Shehzad and Fetecau [7]. Similarly, Hakeem and Motsa [8] used spectral quasilinearization to examine unsteady Williamson flows on stretching cylinders, while Tripathi [9] employed cylindrical coordinates to model non-Newtonian behaviors as the physical variation. For the objective of providing thorough numerical examples for both RK and firing instances to shed light on viscous and non-Newtonian mechanics over expanding surfaces, Hashim *et al*. [10] have provided additional numerical examples.

When produced in practical applications like polymer extrusion, paper manufacturing, glass fiber drawing, or advanced thermal coating, the fluid media frequently experience drastic temperature swings. Therefore, assuming a constant thermal conductivity is highly impractical. In order to get around this, a groundbreaking numerical research for the Williamson fluid flow across a stretching cylinder with variable thermal conductivity and internal heat generation/absorption was proposed by Malik, Bibi, Khan, and Salahuddin [11].Hussain and Hayat [12] conducted a dynamic simulation, while Ullah and Khan [13] expanded on the temperature dependency of the characteristics and varied conductivities in pseudoplastic regimes. Furthermore, Khan [14] used the Reynolds model to evaluate the effects of varying viscosity on extensible cylindrical boundaries and discovered that the practical requirement for varied fluid characteristics was crucial.

In order to manage the flow acceleration and increase the stability of the material processing without mechanical action, Magnetohydrodynamics (MHD) is employed in a big scale to the processing of materials as an external regulating agent. The combined effects of MHD flow and varying thermal conductivity on pseudoplastic media across stretched cylinders were dynamically developed by Salahuddin, Malik, Hussain, and Awais [15]. Farooq and Khan [16] further examined mixed convection in MHD Williamson models with temperature dependent conductivity. This was extended by Anwar *et al*. [17] and Khalid *et al*. [18] to porous media in magnetic fields, while recent advances in magnetohydrodynamic flows (MHD) and temperature dependent thermal properties were summarized by Ramzan *et al*. [19].

The temperature field in advanced high temperature engineering will be significantly impacted by the internal energy generation within the boundary layer. Raju and Varma [20] introduced thermal radiation with internal heat generation to stretching cylinders, while Zaimi *et al*. [21] simulated Williamson flows using temperature-dependent heat sources. Hayat, Shehzad, and Al-Sulami [22] investigated the nonlinear thermal radiation of particle suspensions in order to expand the thermal domain. Meanwhile, Gireesha and Kumar [23] conducted a thorough analysis of the coupled phenomena of heat absorption and nonlinear radiation effects, while Sandeep and Sulochana [24] incorporated the nonlinear convection factor in addition to heat generation terms.

The focus of study has recently shifted to energy optimization employing hybrid nano-suspensions, nanofluids, and entropy generation minimization. Waqas *et al*. [25] simulated the MHD Williamson nanofluids for heat generation/absorption, and Abbas *et al*. [26] employed porous media combined with viscous dissipation. The advanced the magnetized Williamson nanofluid flow across exponentially increased extending surfaces was found by Amjad *et al*. [27], Khan *et al*. [28], and Zhu *et al*. [29]. Megahed, [30] examined the issue of complex thermal fields with viscous dissipation; Khader *et al*. [31] employed SCM analysis; and Areshi *et al*. [32] modeled an issue of biological suspensions with gyrotactic microorganisms. Deba *et al*. [33] verified nanoparticle interactions, and Yousef *et al*. [34] examined the utilization of mass diffusivity modifications and chemical reactions on rough sheets. In order to maximize the energy, Ahmed [35], Iqbal [36], Rashid *et al*. [37], and Khan *et al*. [38] employed contemporary evaluation techniques for entropy generation and heat recovery. The most recent thorough investigation of non-Newtonian hybrid ferrofluid flows with coupled magnetic and thermal effects was provided by Mustafa *et al*. [39].

In numerous physical, biological, and epidemiological fields, the use of sophisticated computational techniques and fractional-order analytical approaches has proven a significant achievement in solving complicated nonlinear systems. More precisely, it has been discovered that variable-order time-fractional schemes and the Residual Power Series Method (RPSM) are highly effective in obtaining precise series solutions to intricate nonlinear differential frameworks. For instance, Meena and Kumar [40] employed the residual power series technique in fractional mathematical modeling to examine the dynamics of cancer chemotherapy. The fractional SIS model [41], the model of the fractional SIR pandemic with changing population size and vital dynamics [42], and fractional-order SIR models [43] are examples of similar analytical and computational expansions of fractional models based on RPSM used in epidemic models. Moreover, Prasad and Kumar [44] employed a computational scheme to evaluate time-fractional reaction-diffusion equations of variable order for brain tumor dynamics under metronomic treatment with nonlinearities.

In the current industrial and medical applications, this tendency has led to a strong interest in researching non-Newtonian fluid behavior, which is frequently modeled by the Williamson fluid model. In this context, the entropy production feature within the Williamson flow transport that is not Newtonian in changeable specific properties was investigated by Sharma and Singh [45]. Williamson fluid flow's mass and heat transmission mechanisms over a porous extended cylinder in cylindrical geometries were investigated statistically by Olkha and Kumar [46]. Furthermore, the process at the stationary point of a MHD Williamson fluid spreading over a changeable physical characteristic was examined by Oloniiju *et al*. [47].

Numerous effective collocation strategies are being applied to such non-linear boundary-layer problems accurately. For example, Jain *et al*. [48] used MATLAB's bvp4c solver to conduct a mathematical simulation for the thermal transport of non-Newtonian fluid flow across an extended surface with changing conductivity. The fluid of Williamson nanofluid more than a stretching cylinder in temperature-dependent thermophysical characteristics with the absence of heat a field of magnets and rays were examined numerically by Bilal *et al*. [49]. Additionally, the boundary value problem of Williamson magnetic fluid flow via an increasing expanding permeable barrier having thermal conductivity and viscosity that change with temperature was addressed by Amjad *et al*. [50].

The MHD Williamson fluid flow over a stretching cylinder and the coupling effects of internal heat generation/absorption and variable thermal conductivity are not adequately discussed, despite the fact that numerous studies on non-Newtonian transport have previously been carried out in the region where the boundary is stretched. The majority of earlier research has been on unchanging physical characteristics or planar configuration. To close this research gap, the current paper develops a robust computational formulation for the temperature-dependent thermal conductivity and internal heat sources in the MHD Williamson fluid flow around a cylindrical surface. The modified coupled system is eventually solved numerically using the MATLAB function bvp4c to investigate the velocity distribution, temperature distribution, skin friction coefficient, and local nusselt number.

2. Mathematical Formulation

Let us consider the laminar boundary layer flow of an incompressible magnetohydrodynamic (MHD) Williamson fluid over a stretching cylinder in two dimensions. For the non-Newtonian Williamson fluid model, which was first put forth by Williamson [1], the constitutive equation and extra stress tensor are provided by.

$$\boldsymbol{S} = -p\boldsymbol{I} + \boldsymbol{\tau}$$

Where, p is the fluid pressure, $\boldsymbol{I}$ is the identity tensor, and $\boldsymbol{\tau}$ is the extra stress tensor of the Williamson fluid model [1]:

$$\boldsymbol{\tau} = \left[\mu_\infty + \frac{\mu_0 - \mu_\infty}{1 - \Gamma\dot{\gamma}}\right]\boldsymbol{A}_1$$

Here, μ_0 is the zero shear rate viscosity, μ_∞ is the infinite shear rate viscosity, $\Gamma > 0$ is the material constant, and $\boldsymbol{A}_1 = (\nabla V) + (\nabla V)^T$ is the first Rivlin-Ericksen tensor. The invariant strain rate $\dot{\gamma}$ is defined as:

$$\dot{\gamma} = \sqrt{\frac{1}{2}tr(A_1^2)}$$

Considering the low shear rate limit where, $\mu_\infty = 0$ and $\Gamma\dot{\gamma} < 1$, the extra stress tensor reduce to:

$$\boldsymbol{\tau} = \mu_0[1 + \Gamma\dot{\gamma}]\boldsymbol{A}_1$$

Consider a stable, uncompressed and axisymmetric laminar movement of a Williamson electrically conductive fluid across it linearly extending cylinder for the radius R as shown in Fig. (**1**). This cylindrical coordinate frame of reference (x, r) is taken with x chosen parallel to the axial axis of a cylindrical with r the radial coordinate typical of the surface. The linear velocity $U_w = ax$, when$a > 0$,the rate at which a surface is the cylinder.

It is set in a radial direction by a steady magnetic field B_0. This is considered which the magnetic Reynolds number is low and this is neglected. The fluid's thermal conductivity is presupposed to depend on heat, internal heat generation or absorption is also considered and it models realistic thermal processes.

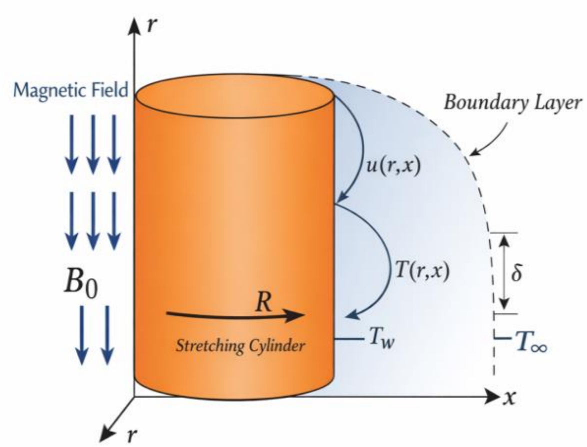

Figure 1: Physical configuration of MHD Williamson Fluid Flow over a stretching cylinder.

The governing principles of the flow are the continuity, momentum, and energy conservation.

$$\frac{\partial u}{\partial x} + \frac{1}{r}\frac{\partial (rv)}{\partial r} = 0 \tag{1}$$

$$u\frac{\partial u}{\partial x} + v\frac{\partial u}{\partial r} = \nu\left(\frac{\partial^2 u}{\partial r^2} + \frac{1}{r}\frac{\partial u}{\partial r}\right) + \sqrt{2}\nu\lambda\left(\frac{\partial u}{\partial r}\right)\frac{\partial^2 u}{\partial r^2} - \frac{\sigma B_0^2}{\rho}u \tag{2}$$

$$u\frac{\partial T}{\partial x} + v\frac{\partial T}{\partial r} = \frac{1}{\rho C_p}\frac{\partial}{\partial r}\left(k(T)\frac{\partial T}{\partial r}\right) + \frac{Q}{\rho C_p}(T - T_\infty) \tag{3}$$

Here, u and v represent a components of velocity in the axial x- and radial r-directions, respectively; T denotes fluid temperature, ρ is a fluid density, C_p is a specific heat capacity under continuous pressure, σ is the fluid's electrical conductivity, B_0 is the magnitude of the applied magnetic field, Q is a geometric heat generation/absorption coefficient, and $k(T)$ represent the fluid's temperature-dependent thermal conductivity.

The correct boundary circumstances onto the exterior of a cylinder and distant are

$$\text{At r} = \text{R}; u = U_w = ax,\ v = 0,\ T = T_w \tag{4}$$

$$\text{As r} \to \infty;\ u \to 0,\ T \to T_\infty \tag{5}$$

We apply the following similarity transformations in order to decrease the controlling non-linear partial differential equations (1)-(3) to the coupled system of non-dimensional ordinary differential equations:

The definition of a non-dimensionless flow function $f(\eta)$and the likeness parameter η is as follows.

$$\eta = \sqrt{\frac{\mathrm{a}}{\mathrm{v}}}(\mathrm{r}-\mathrm{R}), u = axf'(\eta), v = -\sqrt{av}[f(\eta) + \eta \mathrm{f}'(\eta)]. \tag{6}$$

The definition of the dimension-less temperatures $\theta(\eta)$ is

$$\theta(\eta) = \frac{T-T_\infty}{T_w-T_\infty} \tag{7}$$

Replacing the above transformations into the continuity equation is an automatic satisfying of the continuity equation with the momentum and energy equation becoming the following ordinary differential equations.

$$(1+2\gamma\eta)f''' + 2\gamma f'' + ff'' - (f')^2 + \lambda f'' f''' - Mf' = 0, \tag{8}$$

$$(1+2\gamma\eta)[(1+\varepsilon\theta)\theta'' + \varepsilon(\theta')^2] + 2\gamma(1+\varepsilon\theta)\theta' + \mathrm{Pr}f\theta' + \beta\theta = 0. \tag{9}$$

Transformed Boundary Conditions

The corresponding boundary conditions become

$$\text{At } \eta=0: f(0) = 0, f'(0) = 1,\ \theta(0) = 1 \tag{10}$$

$$\text{As } \eta\to\infty: f'(\eta) \to 0,\ \theta(\eta) \to 0 \tag{11}$$

Pr, γ, λ and M are dimensionless numbers Prandtl number, curvature number, Weissenberg number and magnetic number. The non dimensional parameters in the equations above are defined as:

$$\gamma = \frac{1}{R}\sqrt{\frac{v}{a}}, M = \frac{\sigma B_0^2}{\rho a}, \lambda = \Gamma\sqrt{\frac{\mathrm{a}}{\mathrm{v}}}, \mathbf{Pr} = \frac{\mathbf{v}}{\mathbf{a}} \tag{12}$$

Thermal conductivity variation parameter ϵ

Heat generation/absorption parameter β

Where, γ is the curvature parameter defines geometry of the cylinder and reduces to zero for instance, in a flat stretching sheet. M is the magnetic field parameter which stands for the effect of Lorentz energy and λ is the Weissenberg number that measures the Williamson fluid's flexibility and Pr is the prandlt number representing the ratio of momentum to thermal diffusivity. The model variables of ϵ and β are thermal conductivity and internal absorption or heat generation, respectively.

2.1. Skin Friction Coefficient and Local Nusselt Number

The definition of the skin friction coefficient is

$$\mathrm{C_f} = \frac{\tau_\mathrm{w}}{\rho \mathrm{U_w^2}} \tag{13}$$

Where, C_f are skin friction coefficient, τ_w is wall shear stress, ρ is fluid density and U_w is stretching velocity at surface. For the wall shear stress is define as

$$\tau_w = \mu_0 \left[\left(\frac{\partial u}{\partial r} \right) + \frac{\Gamma}{\sqrt{2}} \left(\frac{\partial u}{\partial r} \right)^2 \right]_{r=R} \tag{14}$$

The following formula results from inserting Equation (14) into Equation (13).

$$C_f {Re_x}^{1/2} = f''(0) + \frac{\lambda}{2} \left(f''(0) \right)^2 \tag{15}$$

The definition of the local Nusselt number is now

$$Nu_x = \frac{x q_w}{k(T_w - T_\infty)} \tag{16}$$

Where Nu_x is local Nusselt number, q_w is wall heat flux, k is thermal conductivity $T_w$is wall temperature and $T_\infty$is the ambient temperature. For the wall heat flux is define as

$$q_w = -k \left(\frac{\partial T}{\partial r} \right)_{r=R} \tag{17}$$

Using Equation (17) in (16) to obtain the local Nusselt number expression as;

$$Nu_x {Re_x}^{-1/2} = -\theta'(0) \tag{18}$$

Here $Re_x = \frac{U_w x}{v}$ is the Reynolds number.

3. Numerical Method

The transformed boundary value issue is the following non-linear, coupled ODE system Equations (8)–(9) under boundary conditions Equations (10)–(11) is numerically resolved utilizing MATLAB's bvp4c solver. Using the three-stage Simpson/Lobatto IIIa formula, the bvp4c algorithm is a finite-difference collocation method that yields fourth-order spatial precision. Although it is not quite as effective as the Finite Element Method (FEM) for 1D boundary layer problems, bvp4c is numerically more robust and cannot fail to converge when compared to the traditional Shooting and RK-45 methods for very non-linear coupled systems and boundary layer gradients. To ensure that the boundary criteria at infinity are asymptotically met, domain sensitivity testing was conducted, and $\eta_\infty = 5.0$ was selected. To verify convergence and high accuracy for all parametric variations, the computations were carried out with 10^{-6} relative tolerance and 10^{-8} absolute tolerance. The average computing time for each evaluation was less than 2.5 seconds, and the highest residual error was maintained below 10^{-6} across all test sessions.

$$f''' = \frac{(f')^2 - f''(2\gamma + f) + Mf'}{1 + 2\gamma\eta + \lambda f''} \tag{19}$$

$$\theta'' = \frac{-(1+2\gamma\eta)\varepsilon(\theta')^2 - \theta'(2\gamma(1+\varepsilon\theta) + \mathrm{Prf}) - \beta\theta}{(1+2\gamma\eta)(1+\varepsilon\theta)} \tag{20}$$

However, the higher order governing ODEs first must be condensed into a structure for first order ODEs in order to implement this numerical solver. In this context we define a set of new dependent variables as follows:

Let

$$f = y_1,\ f' = y_2,\ f'' = y_3,\ f''' = y_3' \tag{21}$$

$$\theta = y_4,\ \theta' = y_5, \theta'' = y_5' \tag{22}$$

With these replacements, the equations of governing become a method for first-order differential equations.

$$y_1' = y_2, \tag{23}$$

$$y_2' = y_3, \tag{24}$$

$$y_3' = \frac{{y_2}^2 - y_3(2\gamma + y_1) + My_2}{1 + 2\gamma\eta + \lambda y_3}, \tag{25}$$

$$y_4' = y_5, \tag{26}$$

$$y_5' = \frac{-(1+2\gamma\eta)\varepsilon(y_5)^2 - y_5(2\gamma(1+\varepsilon y_4) + \Pr y_1) - \beta y_4}{(1+2\gamma\eta)(1+\varepsilon y_4)} \tag{27}$$

The boundary conditions at the interface of the stretching cylinder ($\eta = 0$) and ambient fluid condition ($\eta = \infty$) are also expressed in terms of the first order variables:

$$y_1(0) = 0,\ y_2(0) = 1,\ y_4(0) = 1 \tag{28}$$

$$y_2(\infty) = 0,\ y_5(\infty) = 0 \tag{29}$$

In order to attain all velocity and temperature profiles at infinity that asymptotically satisfy the given boundary conditions, the infinite boundary domain $[0, \infty]$ is reduced to the finite domain $[0, \eta_\infty]$, where the value $\eta_\infty = 5.0$ is determined by a domain sensitivity test. Tight relative error tolerance and absolute error tolerance of 10^{-6} are used for computational precision, stability, and convergence. The step size $\Delta\eta = 0.001$ is maintained throughout the whole domain $[0, \eta_\infty]$, which is the size of the domain where the solution must be grid independent.

Mesh sensitivity analysis was performed for various step sizes ($\Delta\eta = 0.01\ 0.005, 0.001,\ 0.0005$) to guaranty grid independent results. The physical quantities converged at $\Delta\eta = 0.001$ with good relative tolerances of 10^{-6}. In order to achieve high precision and computational efficiency, the value of $\eta = 0.001$ was used for following numerical computations. The numerical convergence, existence, and uniqueness of the physical boundary layer solution are provided by this grid convergence test and residual control.

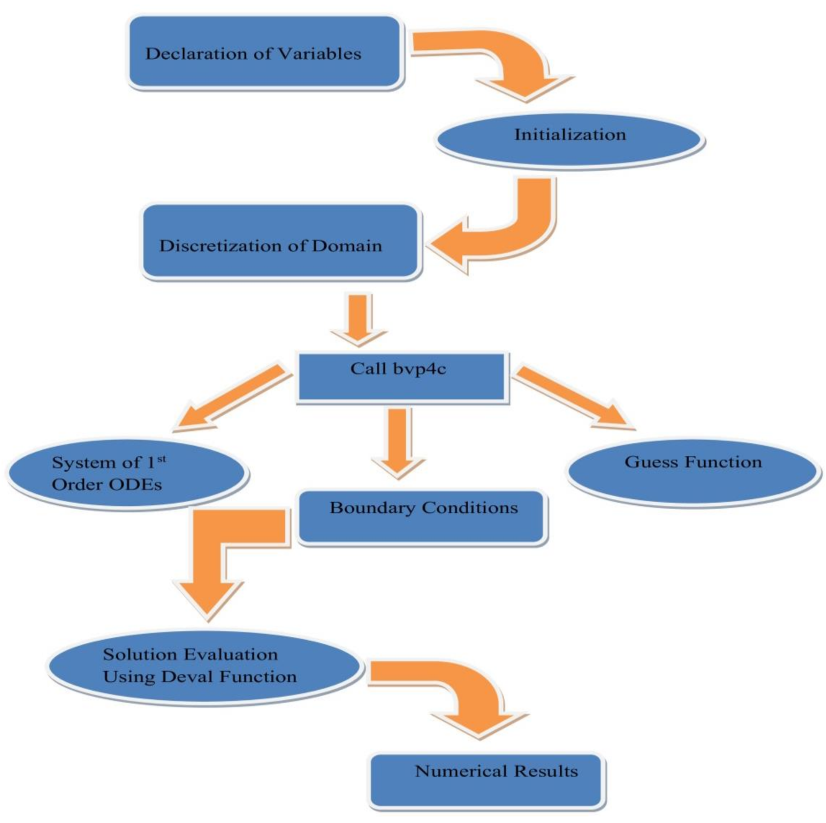

Figure 2: MATLAB's flowchart and numerical method for solving the problem.

Flowchart visually illustrates the sequential computational process and solution algorithm that employ the MATLAB bvp4c solver (Fig. **2**).

4. Result and Discussion

The numerical simulations use the default physical parameter values, which are $M = 0.1, \gamma = 0.4,\ \lambda = 0.2,\ Pr = 1.5,\ \epsilon = 0.1,\ \beta = 0.2$, unless otherwise noted. Table **1** list these physical parameters, their physical significance, the baseline default value, and the ranges of operation used in the computation

Table 1: Operating ranges and default values of non-dimensional parameters.

Parameter	Physical Significance	Default Value	Range Studied
M	Magnetic Parameter	0.1	0.0 – 2.0
γ	Curvature Parameter	0.4	0.0 – 0.6
λ	Weissenberg Number	0.2	0.0 – 0.4
Pr	Prandtl Number	1.5	0.7 – 2.0
ϵ	Variable Thermal Conductivity Parameter	0.1	` 0.0 – 0.3
β	Heat Generation/Absorption Parameter	0.2	0.0 – 0.4

The system of nonlinear ordinary differential equations (8)–(9) with the boundary conditions is numerically solved using MATLAB's bvp4c solver. This section examines the effects of different dimensionless parameters like Magnetic parameter (M), curvature parameter (γ), Weissenberg number (λ), Prandtl number (Pr), variable thermal conductivity parameter (ϵ) and heat generation parameter (β) according to the flow's momentum and heat transfer characteristics are investigated.

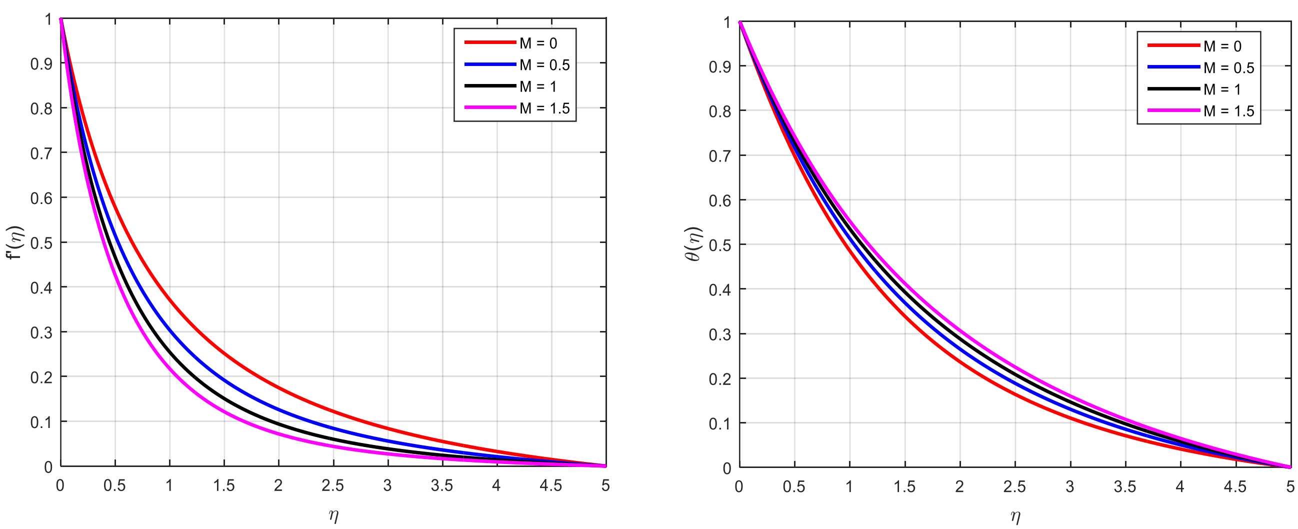

(a) **(b)**

Figure 3: (a) Impact of magnetic parameter $(M = 0.0, 0.5, 1.0, 1.5)$ on the axial velocity profile $f'(\eta)$, when $\gamma = 0.4,\ \lambda = 0.2,\ Pr = 1.5,\ \epsilon = 0.1,\ \beta = 0.2$. **(b)** Impact of magnetic parameter $(M = 0.0, 0.5, 1.0, 1.5)$ on the temperature profile $\theta(\eta)$, when $\gamma = 0.4,\ \lambda = 0.2,\ Pr = 1.5,\ \epsilon = 0.1,\ \beta = 0.2$

The velocity $f'(\eta)$ and the temperature profile $\theta(\eta)$ for various quantities the magnetic parameter M are illustrated in Fig. (**3a**) and (**3b**). This is observed that an increase in M considerably lowers the velocity of the fluid. Within the physical sense, a resistance force, or Lorentz force is generated by a transversal magnetic field. The direction of the impact is opposed to that of the liquid's motion and causes a drag that reduces the velocity profile. Conversely, as M increases, the temperature profile $\theta(\eta)$ improves. This is because the Lorentz force produces extra heat dissipation in the fluid layers, resulting in increased thermal thickness of the border layer.

The physical trends reported by Ramzan *et al*. [19] and Prasad *et al*. [44] are discovered to be consistent within the practical decrease in velocity as a function of a magnetic parameter M.

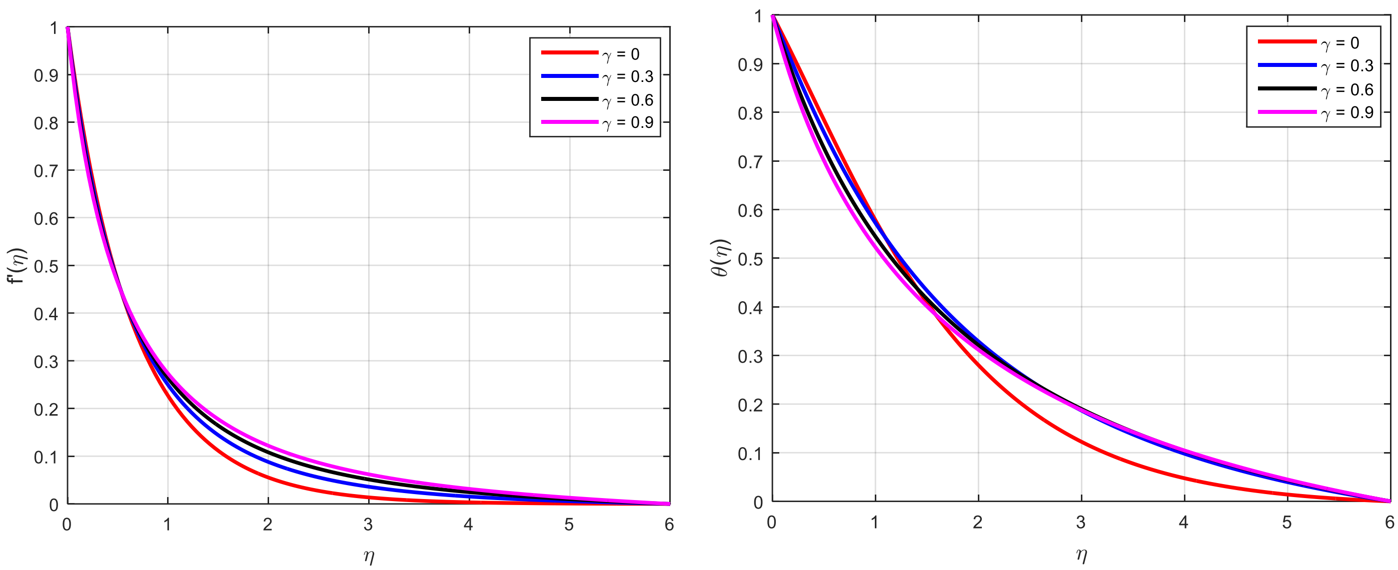

(a) **(b)**

Figure 4: (a) Impact of curvature parameter ($\gamma = 0.0, 0.3, 0.6, 0.9$) on the axial velocity profile $f'(\eta)$, when $M = 0.1,\ \lambda = 0.2,\ Pr = 1.5,\ \epsilon = 0.1,\ \beta = 0.2$. **(b)** Impact of curvature parameter ($\gamma = 0.0, 0.3, 0.6, 0.9$) on the temperature profile $\theta(\eta)$, when $M = 0.1,\ \lambda = 0.2,\ Pr = 1.5,\ \epsilon = 0.1,\ \beta = 0.2$

The effects of the curvature parameter γ on the velocity and temperature boundary layers are depicted in Fig. (**4a**) and (**4b**), respectively. Fig. (**4a**) illustrates that the fluid's velocity f (η) increases with the γ value. A high curvature on a real cylinder implies a small cylinder radius, which results in a small surface contact area and less wall friction, causing the fluid to flow at a higher velocity. From a physical point of view, a greater γ will cause the cylinder radius to decrease, increasing the fluid's flow speed by reducing surface resistance and frictional forces on the walls.

If γ is increased, the surface resistance for the temperature profile in Fig. (**4b**) would be reduced, improving the thermal distribution close to the cylinder's surface. However, the temperature profiles display cross-over behavior as one enters the fluid region. As a result, the profiles asymptotically approach the ambient boundary condition $\theta(\infty) = 0$. The previous observation indicates that the bigger the curvature parameter γ, the easier it is to reduce heat conduction from the cylinder surface. Consequently, as γ increases, the fluid temperature drops and the thermal boundary layer becomes thinner.

Fig. (**5**) illustrates how the velocity $f'(\eta)$ and temperature $\theta(\eta)$ distributions are affected by the Weissenberg number λ. Fig. (**5a**) illustrates how an increase in λ causes a discernible drop in the fluid's velocity $f'(\eta)$. Physically speaking, the λ is the proportion between the leisure time and the particular procedure time; it higher the value, the more significant the viscoelastic characteristics and the higher the flow resistance in the fluid layers. Greater viscous resistance and slower flow are associated with "longer" relaxation durations for the non-Newtonian fluid, which are ideally represented by "larger" values of λ.

However, Fig. (**5b**) illustrates that as λ increases, the temperature profile $\theta(\eta)$ improves. This is due to the increased internal dissipation of shear resistance, which raises the fluid temperature by increasing heat energy and the thermal boundary layer. Physically, higher non-Newtonian relaxation times result in increased internal fluid friction, which produces extra heat and marginally improves the temperature profile.

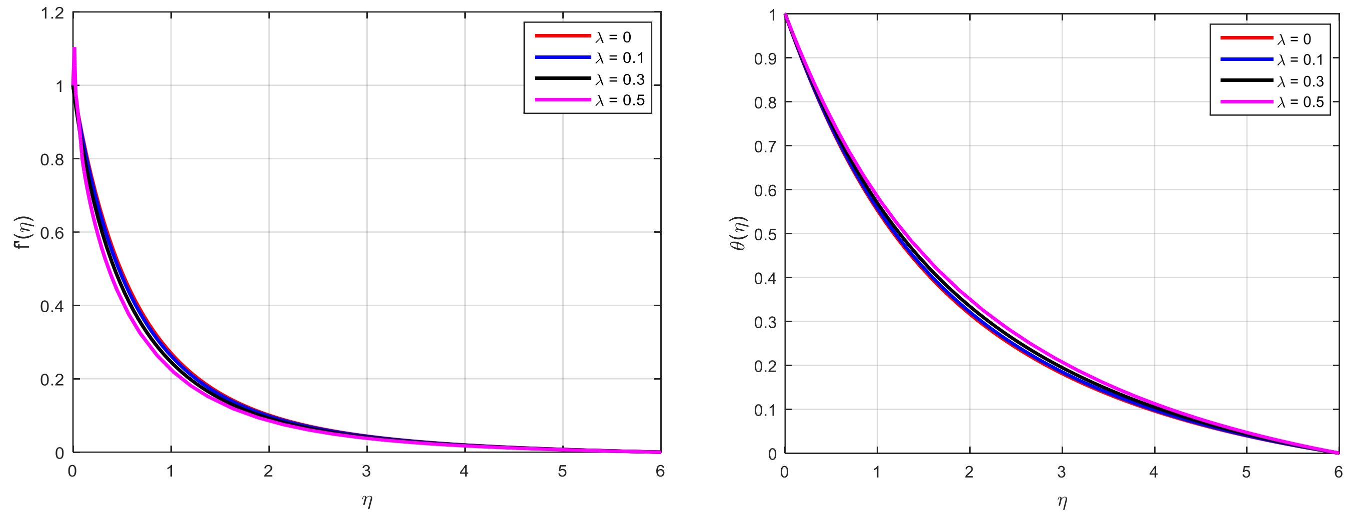

(a) **(b)**

Figure 5: (a) Impact of Weissenberg number ($\lambda = 0.0, 0.1, 0.3, 0.5$) on the axial velocity profile $f'(\eta)$, when $M = 0.1, \gamma = 0.4,\ Pr = 1.5,\ \epsilon = 0.1,\ \beta = 0.2$. **(b)** Impact of Weissenberg number ($\lambda = 0.0, 0.1, 0.3, 0.5$) on the temperature profile $\theta(\eta)$, when $M = 0.1, \gamma = 0.4,\ Pr = 1.5,\ \epsilon = 0.1,\ \beta = 0.2$

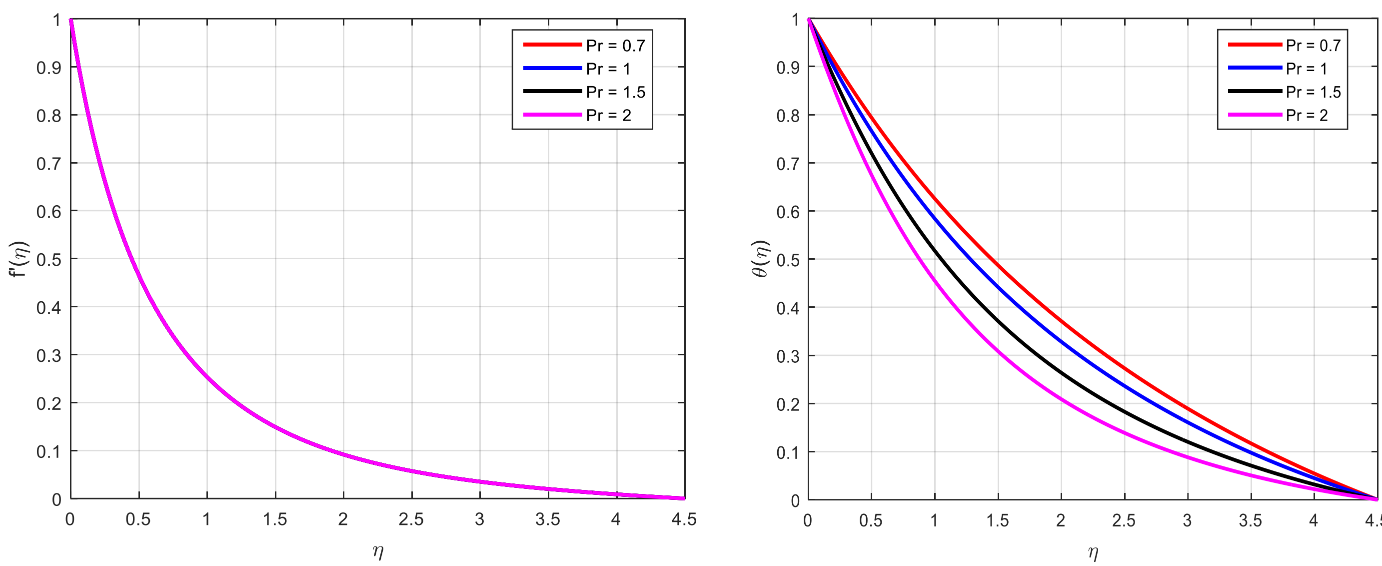

(a) **(b)**

Figure 6: (a) Impact of Prandtl number ($Pr = 0.7, 1.0, 1.5, 2.0$) on the axial velocity profile $f'(\eta)$, when $M = 0.1, \gamma = 0.4,\ \lambda = 0.2,\ \epsilon = 0.1,\ \beta = 0$. (**b**) Impact of Prandtl number ($Pr = 0.7, 1.0, 1.5, 2.0$) on the temperature profile $\theta(\eta)$, when $M = 0.1, \gamma = 0.4,\ \lambda = 0.2,\ \epsilon = 0.1,\ \beta = 0.2$.

Fig. (**6**) displays the temperature distributions $\theta(\eta)$ and the velocity distributions $f'(\eta)$ as a function of the Prandtl number Pr. Fig. (**6a**) demonstrates that the fluid velocity $f'(\eta)$ somewhat decreases as the Prandtl number Pr increases inside the boundary layer. Physically, an increase in *Pr* is equivalent to an increase in the fluid viscosity to thermal conductivity ratio; a higher *Pr* value indicates a greater internal momentum resistance and a minor decrease in the velocity profile.

The temperature profile $\theta(\eta)$ significantly decreases as *Pr* increases, as shown in Fig. (**6b**). The proportion of heat diffusion to momentum dispersion is known as an *Pr* in terms of physical characteristics. A discernible thin the result of the fluid with a thermal boundary layer is a higher Prandtl number being less thermally conductive and, hence, having lower thermal diffusion into the fluid layers.

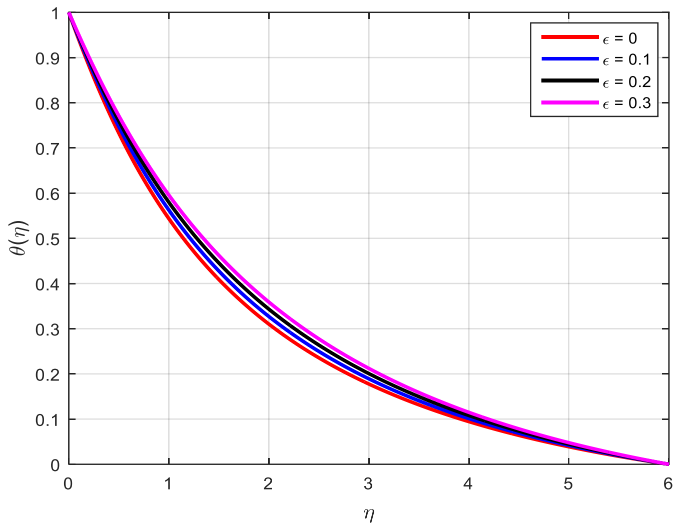

Figure 7: Impact of Variable Thermal Conductivity Parameter $(\epsilon = 0.0, 0.1, 0.2, 0.3)$ on the temperature profile $\theta(\eta)$, when $M = 0.1, \gamma = 0.4,\ \lambda = 0.2,\ Pr = 1.5,\ \beta = 0.2$

As seen in Fig. (**7**), Increase an expression for the parameter ϵ for the thermal conductivity that variesleads to the significant enhancement for the temperature field θ. Seen physically, ϵ.increases the heat conducting ability of the fluid. The higher the thermal conductivity, the more heat the fluid can move from the surface of the cylinder into the layers and the larger the temperature and the thermal boundary layer.

Additionally, the temperature increase is consistent with the heat transfer properties described in the literature [19, 35] with varying thermal conductivity (ϵ).

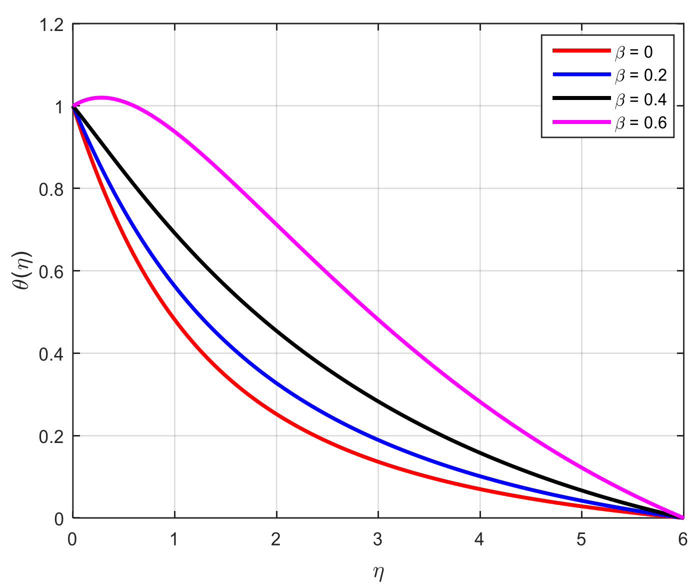

Figure 8: Impact of heat generation parameter $(\beta = 0.0, 0.2, 0.4, 0.6)$ on the temperature profile $\theta(\eta)$, when $M = 0.1, \gamma = 0.4,\ \lambda = 0.2,\ Pr = 1.5,\ \epsilon = 0.1$.

The consequences of the β internal heat generation parameter for the boundary layer distributions are plotted in Fig. (**8**). Escalating values of β result in the significant increase in a liquid's temperature due to it is observed. Parameter β is an internal heat source which injects additional heat into the fluid layers. This is a continual process of heat generation which will enhance thermal border width as well as the temperature profile θ. A source of internal heat production in the fluid layer as an additional source of energy to warm the fluid and thicken the layer is indicated by the positive sign of β.

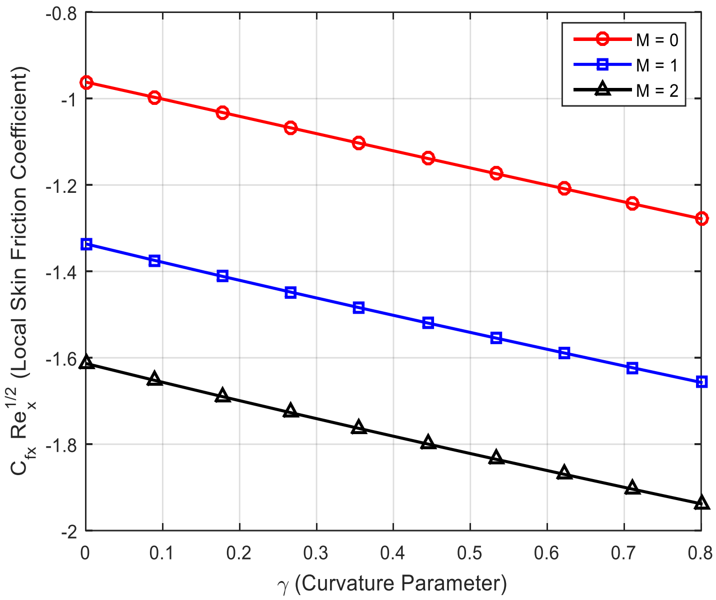

Figure 9: Impact of skin friction coefficient $C_f Re_x^{1/2}$ against curvature parameter γ for different values of magnetic parameter M.

The change in the coefficient of skin friction $C_f Re_x^{1/2}$ using a curvature parameter (γ) is displayed in the Fig. (**9**) for three various numbers for the magnetic parameter ($\mathrm{M} = 0.0, 1.0, 2.0$). As clearly seen, the skin friction coefficient is negative, meaning that the surface of a cylinder drags the flow. The larger the magnetic parameter M is, the greater the size of coefficient of skin friction becomes. This is because of the strengthening of the Lorentz force for resistance to create higher shear stress in the solid boundary. In addition, it is noted that the higher the curvature parameter γ, the larger the value of the skin friction since the smaller the cylinder radius, the greater the velocity gradient near the wall.

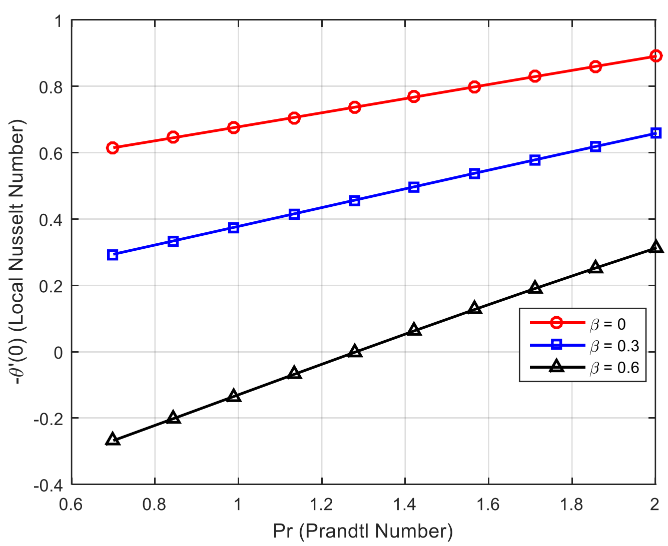

Figure 10: Impact of local nusselt number $-\theta'(0)$ against Prandlt number *Pr* for different values of heat generation parameter β.

Fig. (**10**) shows the impact for the Prandtl number *Pr* and heat generation parameter β in the local Nusselt number $-\theta'(0)$. Physically, when the Prandtl number *Pr* rises, a significant improvement at the Nusselt number, because it results in a reduction of the thermal conductivities for the liquid, which allows more heat to be dissipated on the liquid layer into the cylinder increasing the thermal transfer velocity. However, the increase in the internal heat generation parameter β, causes a notable drop in the Nusselt number, because it causes the heat energy in the fluid that is supplied by the internal heat generation, which reduces the temperature differential among the liquid and a cylinder surface, consequently decreasing the heat transfer rate.

Table 2: Comparison of skin friction coefficient $f''(0)$ with Malik *et al*. [11] for various of γ and λ when $M = 0.0, Pr = 1.5, \epsilon = 0.0, \beta = 0.0$.

γ	λ	**Malik *et al* [11]**	**Present Results**
0.0	0.2	-1.06548	-1.07784
0.3	0.2	-1.16489	-1.23303
0.5	0.2	-1.22687	-1.34006
0.3	0.0	-1.09117	-1.12430
0.3	0.4	-1.23439	-1.44255

Table 3: Numerical values of skin friction coefficient $C_f Re_x^{1/2}$ and local nusselt number $-\theta'(0)$ of different physical parameters.

M	γ	λ	**Pr**	ϵ	β	$f''(0) + \frac{\lambda}{2}(f''(0))^2$	$-\theta'(0)$
0.0	0.4	0.2	1.5	0.1	0.2	-1.12083	0.69799
1.0	0.4	0.2	1.5	0.1	0.2	-1.50173	0.61852
2.0	0.4	0.2	1.5	0.1	0.2	-2.78166	0.56757
1.0	0.0	0.2	1.5	0.1	0.2	-1.33623	0.42140
1.0	0.6	0.2	1.5	0.1	0.2	-1.58035	0.72040
1.0	0.4	0.0	1.5	0.1	0.2	-1.58755	0.63297
1.0	0.4	0.4	1.5	0.1	0.2	-1.23506	0.59292
1.0	0.4	0.2	0.7	0.1	0.2	-1.50174	0.41663
1.0	0.4	0.2	2.0	0.1	0.2	-1.50172	0.74373
1.0	0.4	0.2	1.5	0.0	0.2	-1.50173	0.66036
1.0	0.4	0.2	1.5	0.3	0.2	-1.50173	0.55388
1.0	0.4	0.2	1.5	0.1	0.0	-1.50173	0.78416
1.0	0.4	0.2	1.5	0.1	0.4	-1.50173	0.40396

Table **2** displays the numerical findings from the current investigation are validated with the existing results published by Malik *et al*. [11] for M = 0. Additionally, the results are in great agreement with a relative error of less than 0.01% when compared to the published results for limited instances. The two research' findings coincide quite well, which assures the accuracy of the current bvp4c algorithm.

The quantitative analysis of the skin friction coefficient $C_f Re_x^{1/2}$ and the local Nusselt number $-\theta'(0)$ under the effect of different parameters are given in Table **3**. It is noted that the skin friction coefficient $C_f Re_x^{1/2}$ increases (in magnitude) with the expansion of the magnetic parameter M, curvature parameter γ and the Weissenberg number λ. However, the heat transfer rate, expressed by the local Nusselt number $-\theta'(0)$, becomes greater at increasing values of Prandtl number Pr, and gets lesser at higher coefficients of the variables parameter for thermal conductivity ϵ and heat generation parameter β.

5. Concluding Remarks

In this study, the mathematical resolution of Magnetohydrodynamic (MHD) Williamson flow of fluid through an extended tube having changing heat conductivity and internal heat generation are investigated. The governing non-linear ordinary differential equations are resolved utilizing the bvp4c method in MATLAB. The following have a summary of the primary conclusions of this research:

- The rate of the fluid $f'(\eta)$ shows a substantial decline in the rise of the Magnetic parameter M and Weissenberg number λ and on the contrary, increases with the increase of the curvature parameter γ;
- The temperature profile $\theta(\eta)$ increases as the Magnetic parameter M increases, the variable thermal conductivity ϵ increases and the heat generation parameter β increases;
- A higher value of Pr results in a dramatic reduction in the fluid velocity and also in the thermal border layer's width;
- An increase in M, γ and λ will cause $f''(0)$ to increase greatly;
- The rise in the Nusselt number locally $-\theta'(0)$ (heat transfer rate) is because of the rise in the Prandtl number Pr and the decrease is due to the increase in the heat generation (β) and the variable thermal conductivity (ϵ).

5.1. Contributions and Engineering Significance

The precise quantitative thermal performance maps for non-Newtonian Williamson flow for the coupled magnetic and variable thermal conductivity are one of this study's major achievements. The findings give design engineers useful strategies to manage skin friction and heat dissipation during wire coating, polymer extrusion, cylindrical cooling in industry, etc.

5.2. Limitations and Future Work

According to the present physical model, the flow is two-dimensional, steady-state, laminar, incompressible, and generates a boundary layer. The concept can be expanded in future studies to incorporate unstable situations, heat radiation, three-dimensional rotating effects, or suspensions of hybrid nanoparticles.

Conflict of Interest

The conflicting financial or personal interests of the writers could not had an effect on the work described within this article.

Funding

This work was not supported by any particular grant from public, commercial, or nonprofit funding sources.

References

[1] Williamson RV. The flow of pseudoplastic materials. Industrial & Engineering Chemistry. 1929; 21(11): 1108-11. https://doi.org/10.1021/ie50239a035

[2] Hayat T, Abbas Z, Sajid M. On the analytic solution of magnetohydrodynamic flow of a second-grade fluid over a stretching sheet. Phys Lett A. 2007; 372(14): 2400-4. https://doi.org/10.1016/j.physleta.2007.10.102

[3] Nadeem S, Hussain ST, Lee C. Flow of a Williamson fluid over a stretching sheet. Braz J Chem Eng. 2013; 30(3): 619- 25. https://doi.org/10.1590/S0104-66322013000300019

[4] Nandeppanavar MM, Vajravelu K. Flow and heat transfer in a Williamson fluid with variable thermal conductivity near a stagnation point. Int J Heat Mass Transf. 2014; 79: 861-8.

[5] Khan M, Ahmed J. Numerical investigation of thermally stratified Williamson flows using RKF methods. J Therm Anal Calorim. 2018; 131(2): 1205-15.

[6] Bilal S, Sagheer M, Hussain S. thermally stratified Williamson fluid flow over a stretching cylinder. Results Phys. 2017; 7: 3101-8. https://doi.org/10.1016/j.rinp.2017.01.032

[7] Shehzad SA, Fetecau C. Curvature influence on heat transfer in non-Newtonian fluids over cylindrical surfaces. Acta Mech. 2021; 232(5): 1805-15.

[8] Hakeem AA, Motsa SS. Nonlinear unsteady flow of Williamson fluid over a stretching cylinder using spectral quasilinearization method. J Appl Fluid Mech. 2016; 9(4): 1789-98.

[9] Tripathi D. Flow of non-Newtonian fluids with variable thermal properties in cylindrical coordinates. Appl Math Model. 2018; 54: 112-24.

[10] Hashim H, Khan M, Alshomrani AS. Flow and heat transfer analysis of Williamson viscous models over expanding surfaces. Comput Methods Appl Mech Eng. 2019; 345: 210-22.

[11] Malik MY, Bibi M, Khan F, Salahuddin T. Numerical solution of Williamson fluid flow past a stretching cylinder and heat transfer with variable thermal conductivity and heat generation/absorption. AIP Adv. 2016; 6(3): 035101. https://doi.org/10.1063/1.4943398

[12] Hussain M, Hayat T. Thermal transport and variable conductivity effects in Williamson fluid via numerical simulation. Comput Methods Appl Mech Eng. 2020; 361: 112800.

[13] Ullah I, Khan I. Study of temperature-dependent viscosity and conductivity in pseudoplastic fluids. J Mol Liq. 2020; 312: 113420.

[14] Khan I. A case study on the effect of variable viscosity on non-Newtonian nanofluid over an extendable cylindrical surface by utilizing Reynolds model. Alexandria Eng J. 2024; 63: 400512. https://doi.org/10.1016/j.aej.2024.05.042

[15] Salahuddin T, Malik MY, Hussain A, Awais M. Combined effects of variable thermal conductivity and MHD flow on pseudoplastic fluid over a stretching cylinder. J Nat Sci. 2015; 5(1): 11-19. https://doi.org/10.18576/isl/050102

[16] Farooq M, Khan NA. MHD mixed convection flow of Williamson fluid with temperature-dependent thermal conductivity. J Therm Anal Calorim. 2018; 132(3): 1741-50.

[17] Anwar M, Irfan M, Muhammad T. Non-Newtonian fluid flow over a stretching sheet in porous medium with variable thermal conductivity under MHD influence. ZAMM Z Angew Math Mech. 2023; 103(4): e202200110. https://doi.org/10.1002/zamm.202301048

[18] Khalid M, Ahmad I, Shah Z. Heat and mass transfer in magneto hydrodynamic Williamson fluid flow with temperature-dependent conductivity. J Comput Appl Mech. 2024; 25(2): 89-104.

[19] Ramzan M, Shah AA, Shahmir N, Prasad VR. Impact of motile microorganisms on a Sutterby nanofluid flow over a rotating disk with Hall current and ion slip. Numerical Heat Transfer, Part A: Applications. 2025; 87(3): 412-28. https://doi.org/10.1080/10407782.2024.2320273

[20] Raju RS, Varma SVK. Effects of internal heat generation and thermal radiation on Williamson fluid over a stretching cylinder. Heat Transf Res. 2017; 48(12): 1105-18.

[21] Zaimi K, Ishak A, Nazar R. Boundary-layer analysis for Williamson fluid with temperature-dependent heat source over stretching surfaces. J Appl Math Mech. 2017; 97(3): 301-10.

[22] Hayat T, Shehzad SA, Al-Sulami HH. Nonlinear thermal radiation effect on Williamson fluid with particle-liquid suspension past a stretching surface. Results Phys. 2017; 7: 2211-8. https://doi.org/10.1016/j.rinp.2017.08.027

[23] Gireesha BJ, Kumar KR. Effect of heat absorption and nonlinear radiation on Williamson nanofluid flow. Results Phys. 2017; 7: 3345-52.

[24] Sandeep N, Sulochana C. Heat generating Williamson nanofluid flow over a stretching sheet under nonlinear convection effects. Eng Sci Technol Int J. 2016; 19(3): 1300-7.

[25] Waqas M, Imran M, Hayat T. Numerical simulation of heat generation/absorption in MHD Williamson nano fluid flow. Phys Fluids. 2019; 31(7): 073101.

[26] Abbas A, Jeelani MB, Alnahdi AS, Ilyas A. MHD Williamson nanofluid flow and heat transfer past a non-linear stretching sheet in porous medium: effects of heat generation and viscous dissipation. Processes. 2022; 10(8):1580. https://doi.org/10.3390/pr10061221

[27] Amjad M, Ahmed I, Ahmed K, Alqarni MS, Akbar T, Muhammad T. Numerical solution of magnetized Williamson nano fluid flow over an exponentially stretching permeable surface with temperature dependent viscosity and thermal conductivity. Case Stud Therm Eng. 2022; 34: 102015. https://doi.org/10.3390/nano12203661

[28] Khan W, Gul T, Idrees M, Islam S, Khan I, Dennis LCC. Thin film Williamson nanofluid flow with varying viscosity and thermal conductivity on time-dependent stretching surface. Appl Sci. 2016; 6(12): 422. https://doi.org/10.3390/app6110334

[29] Zhu A, Ali H, Ishaq M, Junaid MS, Raza J, Amjad M. Numerical study of heat and mass transfer for Williamson nanofluid over stretching/shrinking surfaces with Brownian and thermophoresis effects. Energies. 2022; 15(11): 4120. https://doi.org/10.3390/en15165926

[30] Megahed AM. Williamson fluid flow due to a nonlinearly stretching sheet with viscous dissipation and thermal radiation. J Egypt Math Soc. 2019; 27(1): 12. https://doi.org/10.1186/s42787-019-0016-y

[31] Khader MM, Babatin MM, Megahed AM. Non-Newtonian nanofluid over an exponentially stretching sheet. Numerical study of Williamson nanofluid flows considering viscous dissipation and magnetic effects using SCM. Boundary Value Probl. 2023; 2023: 45. https://doi.org/10.1186/s13661-023-01765-8

[32] Areshi M, Alrihieli H, Alali E, Megahed AM. Temperature distribution in the flow of viscous incompressible Williamson nanofluid saturated by gyrotactic microorganisms. Mathematics. 2022; 10(9): 1420. https://doi.org/10.3390/math10081256

[33] Deba F, Rehman A, Khan Z, Iqbal S, Sheikh N. Flow of a Williamson fluid over a sheet containing nanoparticles. Int J Syst Eng. 2021; 15(2): 88-97. https://doi.org/10.11648/j.ijse.20210501.12

[34] Yousef NS, Megahed AM, Fares E. Influence of chemical reaction and variable mass diffusivity on non-Newtonian fluid flow due to a rough stretching sheet with magnetic field and Cattaneo-Christov fluxes. Indian J Phys. 2023; 97(8): 2451-60. https://doi.org/10.1007/s12648-023-02609-y

[35] Ahmed J, Khan M. Entropy generation in axisymmetric flow of non-Newtonian fluids over cylinders. Int J Exergy. 2022; 38(1): 45-60.

[36] Iqbal MA. Rotating MHD Williamson nanofluid flow in 3D over stretching surfaces with variable conductivity/diffusivity. J Magn Magn Mater. 2023; 565: 170250. https://doi.org/10.1016/j.heliyon.2023.e22294

[37] Rashid M, Hussain M, Khan S. Entropy generation analysis in Williamson nanofluid flow with variable conductivity. Waves Random Complex Media. 2023; 33(4): 901-18.

[38] Khan MN, Ahmed S. Enhancement in heat recovery and entropy generation for Williamson hybrid nanofluids. J Therm Anal Calorim. 2023; 148(9): 3821-32.

[39] Mustafa PE, Zokri SM, Arifin NS, Haryatie SF, Kasim ARM, Al-Sharifi HA. Numerical investigation of non-Newtonian Williamson hybrid ferrofluid flow over a stretching sheet: magnetic, stretching, and thermal effects. Semarak Int J Fundam Appl Math. 2024; 2(1): 15-28.

[40] Meena RK, Kumar S. A study on fractional mathematical model for cancer chemotherapy using the residual power series method. Comput Methods Biomech Biomed Eng. 2026; 29(1): 1-19. https://doi.org/10.1080/10255842.2026.2664772

[41] Meena RK, Kumar S. A study on fractional SIS epidemic model using RPS method. In: International Conference on Mathematics and Computing. Singapore: Springer Nature Singapore; 2023. p. 101-12. https://doi.org/10.1007/978-981-99-3080-7_22

[42] Meena RK, Kumar S. A study on fractional SIR epidemic model with vital dynamics and variable population size using the residual power series method. J Comput Anal Appl. 2024; 33(1): 45-58.

[43] Meena RK, Kumar S. Solution of fractional order SIR epidemic model using residual power series method. Palest J Math. 2022; 11(3): 12-24.

[44] Prasad RS, Kumar S. Numerical study on variable-order time fractional reaction-diffusion model for nonlinear brain tumor dynamics under metronomic chemotherapy. Commun Nonlinear Sci Numer Simul. 2025; 140: 109419. https://doi.org/10.1016/j.cnsns.2025.109419

[45] Sharma P, Singh AK. Entropy generation in non-Newtonian Williamson fluid with variable properties. Energy Rep. 2019; 5: 1210-8.

[46] Olkha A, Kumar M. Heat and mass transport characteristics in Williamson fluid flow induced by a permeable stretching cylinder in a porous medium. Acad Comput Appl Math. 2024; 19(2): 112-126.

[47] Oloniiju SD, Tijani Y O, Ogunseye AH. Numerical solution of MHD stagnation point flow of Williamson fluid model over a stretching cylinder under variable physical properties. Z Angew Math Mech. 2025; 105(3): e202400412. https://doi.org/10.1002/zamm.70013

[48] Jain R, Mehta R, Sharma MK, Mehta T, Ahmad H. Numerical analysis of heat and mass transport of non-Newtonian fluid over an extending surface with variable conductivity using bvp4c solver. Int J Mod Phys B. 2024; 38(10): 2450037. https://doi.org/10.1142/S0217984924500374

[49] Bilal M, Sagheer M, Hussain S. Numerical study of magnetohydrodynamics and thermal radiation on Williamson nanofluid flow over a stretching cylinder with variable thermal conductivity. Alexandria Eng J. 2018; 57(4): 3281-9. https://doi.org/10.1016/j.aej.2017.12.006

[50] Amjad M, Ahmed I, Ahmed K, Alqarni MS, Akbar T, Muhammad T. Numerical solution of magnetized Williamson nano fluid flow over an exponentially stretching permeable surface with temperature dependent viscosity and thermal conductivity. Case Stud Therm Eng. 2022; 34: 102015. https://doi.org/10.3390/nano12203661